International Journal of Nanomedicine

Dovepress

open access to scientific and medical research

Open Access Full Text Article

ORIGINAL RESEARCH

# Delivery of siRNAs Against Selective Ion Channels and Transporter Genes Using Hyaluronic Acid-coupled Carbonate Apatite Nanoparticles Synergistically Inhibits Growth and Survival of Breast Cancer Cells

Mohammad Borhan Uddin[1], Mark M Banaszak Holl[2,3], Ezharul Hoque Chowdhury[4,5]

[1]Department of Pharmaceutical Sciences, School of Health and Life Sciences, North South University, Dhaka, Bangladesh; [2]Department of Mechanical and Materials Engineering, School of Engineering, University of Alabama at Birmingham, Birmingham, AL, USA; [3]Division of Pulmonology, Allergy, and Critical Care Medicine, Heersink School of Medicine, University of Alabama at Birmingham, Birmingham, AL, USA; [4]Jeffrey Cheah School of Medicine and Health Sciences, Monash University Malaysia, Subang Jaya, Selangor, 47500, Malaysia; [5]Nanoflex LLC, Leesburg, FL, 34748, USA

Correspondence: Ezharul Hoque Chowdhury, Tel +1 352 409 2283, Email chowdhury@nanoflex-usa.com; Mohammad Borhan Uddin, Tel +880-1974276229, Email mohammad.uddin@northsouth.edu

**Introduction:** Dysregulated calcium homeostasis and consequentially aberrant $Ca^{2+}$ signalling could enhance survival, proliferation and metastasis in various cancers. Despite rapid development in exploring the ion channel functions in relation to cancer, most of the mechanisms accounting for the impact of ion channel modulators have yet to be fully clarified. Although harnessing small interfering RNA (siRNA) to specifically silence gene expression has the potential to be a pivotal approach, its success in therapeutic intervention is dependent on an efficient delivery system. Nanoparticles have the capacity to strongly bind siRNAs. They remain in the circulation and eventually deliver the siRNA payload to the target organ. Afterward, they interact with the cell surface and enter the cell via endocytosis. Finally, they help escape the endo-lysosomal degradation system prior to unload the siRNAs into cytosol. Carbonate apatite (CA) nanocrystals primarily is composed of $Ca^{2+}$, carbonate and phosphate. CA possesses both anion and cation binding domains to target negatively charged siRNA molecules.

**Methods:** Hybrid CA was synthesized by complexing CA NPs with a hydrophilic polysaccharide – hyaluronic acid (HA). The average diameter of the composite particles was determined using Zetasizer and FE-SEM and their zeta potential values were also measured.

**Results and Discussion:** The stronger binding affinity and cellular uptake of a fluorescent siRNA were observed for HA-CA NPs as compared to plain CA NPs. Hybrid CA was electrostatically bound individually and combined with three different siRNAs to silence expression of calcium ion channel and transporter genes, *TRPC6*, *TRPM8* and *SLC41A1* in a human breast cancer cell line (MCF-7) and evaluate their potential for treating breast cancer. Hybrid NPs carrying *TRPC6*, *TRPM8* and *SLC41A1* siRNAs could significantly enhance cytotoxicity both in vitro and in vivo. The resultant composite CA influenced biodistribution of the delivered siRNA, facilitating reduced off target distribution and enhanced breast tumor targetability.

**Keywords:** carbonate apatite, nanoparticles, siRNA, breast cancer, cytotoxicity, hyaluronic acid, calcium ion channel, transporter genes, *TRPC6*, *TRPM8*, *SLC41A1*

## Introduction

Gene therapy generally influences expression of gene in living organisms by delivering either exogenous DNA or RNA for treating different types of cancer diseases. RNA interference (RNAi) is a gene therapy tool. Many studies suggested that this tool has therapeutic potential when either used alone or in conjunction with other treatments.[1,2]

Over the past two decades, there was faster development in evolving the ion channel functions in connection with cancer, but most of their mechanisms on growth, development and prognosis of cancer cells have yet to be fully clarified.

Received: 29 November 2023
Accepted: 25 March 2024
Published: 29 July 2024

Calcium (Ca) channels have great importance as $Ca^{2+}$ is a messenger regulating signalling pathways and also important in cellular processes.[3–6] The cell membrane contains many membrane proteins to control numerous cell signal-transduction pathways and maintain chemical, electrical and mechanical homeostasis of the cell. The constant maintenance of the concentrations of the major inorganic cations and anions is a critical function carried out by the plasma membrane.[4,6,7] Recent studies[8,9] found an association between cancer development/progression and the level of the expression of the magnesium (Mg) transporter genes. Upward regulation of Mg transporters might be connected with carcinogenesis and anticancer drug resistance, therefore these genes might be crucial biomarkers for contributing the development and progression of different type cancer diseases. Ca or Mg ion channels showed either underexpressed or overexpressed in many cancer diseases including breast cancer. These channels might have led to increased efflux of drug, decreased influx of drug, eventually stopping apoptosis and ultimately facilitating tumorigenesis to a greater extent.[2–4]

Ca ion channels in many cases play the role for switching on and off intracellular signalling pathways, making them potential drug targets. They are also mostly expressed on the cell surface. For this reason, these ion channel targeting drugs have some advantages as they do not need to enter the cell. Considering it, members of the transient receptor potential (TRP) channel family, in many recent studies have been proposed as potential biomarkers and/or drug targets in cancer therapy.[8]

Among the TRP channels, *TRPM7*, is a widely researched a Ca and Mg ion channel on its upstream characteristics in malignancy,[10] but inadequate data was found for another ion channel, *TRPM8*.[11–14] Many studies have accumulated results of *TRPM8* expression in cancer cells especially prostate, lung and colorectal cancer, whereas, a very few studies were conducted in breast cancer.[15–17] Chodon et al showed, for the first time, that *TRPM8* protein was overexpressed in human breast adenocarcinomas and this overexpression was specifically correlated with ERα (intracellular estrogen receptor). Moreover, in MCF-7 cancer cell line, the expression of *TRPM8* was regulated by estrogen. Either expression silencing of ER or deprivation of E2 (17-β- estradiol) might have led to decrease in *TRPM8* mRNA expression, thereby suggesting a hormonal regulation in breast cancer.[18]

In the MCF-7 cancer cell line, *TRPC6* was expressed to a greater extent compared to the nearby nontumor cells. TRP channels are seen in the overexpressed stages in breast cancer patients, thereby maintaining both the increased proliferation rate and the enhancing cell survival and providing resistance to apoptosis.[11]

*SLC41A1* was recently identified as a $Na^{+}/Mg^{2+}$ exchanger and established to be linked to a TRP subfamily (such as *TRPM7*) that increased calcium flickers and cell adhesion.[19–22]

Ideal nanoparticles (NPs) loaded with siRNA can remain in the circulation, may be able to deliver the siRNA to the targeted organ, interact with the cell surface, enter the cell and finally, facilitate in freeing the endosome as well as lysosome system to release the siRNAs within the cytoplasm[23–25] Hydrophilic polymers are recently used to increase the solubility and prolong the half-life of inorganic nanoparticles in the plasma. After administration, NPs immediately encounter a dramatic challenge in biological environment. This biological environment consists of various biomolecules that create “protein corona” as a result. Protein corona has roles in nanotoxicology, macrophage recognition, opsonization and cellular internalization of NPs.[26,27]

CD44, a cell-surface multifunctional and multistructural molecule, is involved in cell proliferation, differentiation, migration, as well as angiogenesis.[28–31] As per comparison with normal cells, expression of CD44 was high in many cancer cells. Many studies recognized it as an effective therapeutic target in cancer therapy.[32–36] Hyaluronic acid (HA), a polysaccharide compound, serves as a major component of the extracellular matrix. Having its affinity to specifically target CD44 receptors, HA was widely used with drug nanocarriers in many studies to increase the delivery of the respected drug in CD44-overexpressed tumor cells.[37] HA-modified nanoparticles were used in many recent studies, such as CD44-targeted siRNA delivery to treat bladder cancer,[38,39] codelivery of silver and liposomes for treating cancer,[39] targeted treatment of tumors to overcome multidrug resistance, codelivery of miR34a and anticancer drug doxorubicin in resistant breast cancer,[40] loading an HSP90 inhibitor for subcutaneous and orthotropic colon cancer therapy,[41] targeted delivery of cabazitaxel to CD44-overexpressing glioblastoma cells,[42] oligosaccharide-CD44v6-targeting oxaliplatin for colorectal cancer,[43] codelivery of docetaxel for breast cancer treatment,[44] codelivery of olaparib-PEI - PLGA for targeted therapy of breast cancer,[45] as redox-responsive agent for targeted photodynamic therapy/chemotherapy against breast cancer,[46] loading copper ion and disulfiram for esophageal cancer,[47] targeted delivery of microRNA-125b in pancreatic cancer[48] and selective transport of curcumin in breast and other cancer cells.[49–52]

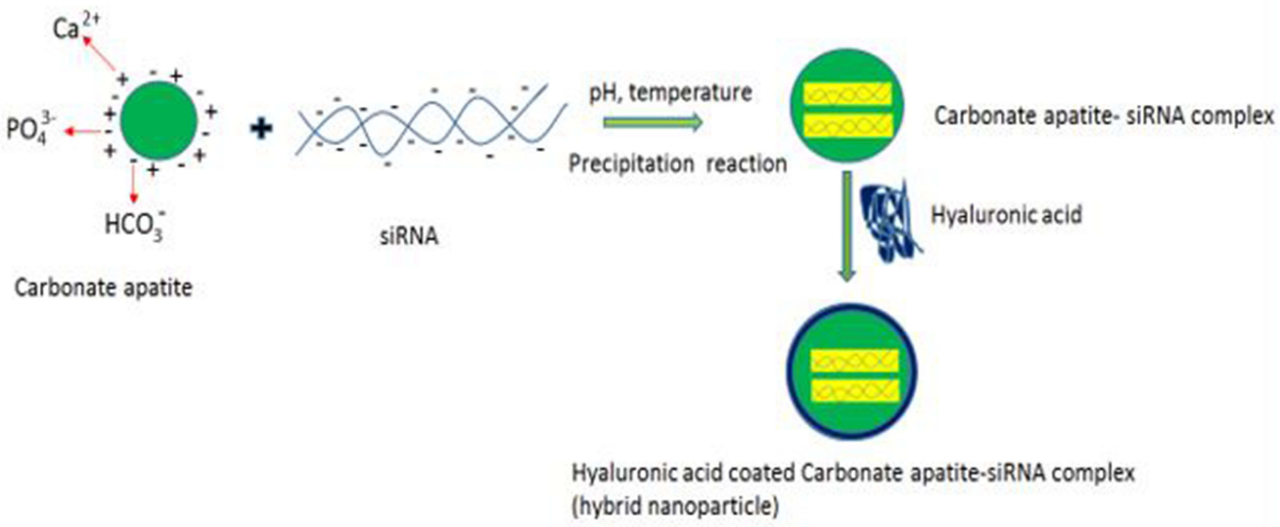


**Figure 1** Molecular mechanism for generation of carbonate apatite hybrid nanoparticle complex with siRNA.[38]

CA particles has got some advantageous points like simplicity to fabricate (Figure 1), biodegradability property and versatility nature compared to the organic counterparts. The fascinating pH sensitive feature and having the core constituents of $Ca^{2+}$, phosphate and bicarbonate which are naturally available in the body, make CA highly biodegradable in nature and potentially safe to be used clinically. In addition, the heterogeneous surface charge distribution enabled it to be a versatile carrier of various chemotherapeutic drugs and genetic materials which bind to it via electrostatic interactions.[53–55] In contrast, an insignificant number of studies have been carried out to date on the roles of Ca ion channels and transporter genes in cellular growth and proliferation of breast cancer. Our previous study conducted a protein analysis by Western blot. The MCF-7 cells were treated with six CA-siRNA complexes. The knockdown of *TRPC6* or a cocktail of siRNAs targeting *TRPC6*, *TRPM8*, and *SLC41A1* delivered into MCF-7 cells with plain CA NPs exhibited the greatest cytotoxicity effects.[7]

# Materials and Methods

## Materials

The materials purchased from Sigma-Aldrich (St Louis, MO, USA) were calcium chloride dihydrate, sodium bicarbonate, Dulbecco's modified eagle medium (DMEM), potassium phosphate monobasic ($KH_2PO_4$), dimethyl sulphoxide (DMSO) and thiazolyl blue tetrazolium bromide (MTT). DMEM powder, fetal bovine serum (FBS), trypsin-ethylenediamine tetraacetate (trypsin-EDTA), penicillin-streptomycin were obtained from Gibco BRL (CA, USA) and hyaluronic acid (HA) (mol wt. 8000–15,000) from Sigma-Aldrich (St Louis, MO, USA). The AF 488 negative siRNA and experimental siRNAs (Table 1)

**Table 1** Genes Targeted by Specific siRNAs from Qiagen

| siRNA (Batch Number) | Targeted Gene (Symbol) | Official Name |
|---|---|---|
| Hs_TRPC6_1 FlexiTube siRNA (SI00066129) | *TRPC6* | Transient receptor potential cation channel, subfamily C, member 6 |
| Hs_TRPM8_1 FlexiTube siRNA (SI00135744) | *TRPM8* | Transient receptor potential cation channel, subfamily M, member 8 |
| Hs_SLC41A1_5 FlexiTube siRNA (SI03242932) | *SLC41A1* | Solute carrier family 41 (magnesium transporter), member 1 |

were bought from QIAGEN (Valencia, CA, USA). Murine breast cancer cell line, 4T1 and human breast cancer cell line, MCF-7 was purchased from ATCC.

## Development of CA NPs and Particle Size Measurement

CA NPs were prepared following previously established protocols.[54] 44 mM, 88 mM and 176 mM of the sodium bicarbonate were separately mixed with the DMEM powder containing endogenous inorganic phosphate (Pi) in miliQ water (pH adjusted to 7.4) This freshly prepared medium (200 µL) was mixed with the different concentrations of exogenous calcium chloride (5,10, 15, 20, 25, 30, 35, 40, 45, and 50 mM), followed by the incubation for at least 30 min at 37°C and afterward medium was added to make the total volume of 1 mL. Then 10% FBS was added to each sample for preventing any kind of aggregation. The concentrations of the inorganic phosphate (Pi) as well as the carbonate ions used to prepare nanoparticles remained fixed at a pH of 7.4. To get the expected particle size range of NPs, the above fabrication step was repeated without 10% FBS to analyze the turbidity of the NPs. At a fixed wavelength of 320 nm using a spectrophotometer, (UV 1800 Spectrophotometer, Shimadzu), the absorbance was measured then immediately after the aforementioned 30 min incubation. To measure the average size of the NPs, the Zetasizer (Nano ZS, Malvern) was used. Before this step, 10% FBS as per protocol was added to the 1 mL of fabricated NPs and the particles were kept on ice. This was to stop particle formation and aggregation. On the Zetasizer, a refractive index of 1.325 was used. Data analysis was carried out using Zetasizer software 6.20 and all measurements were performed in triplicate.

## Modification of NPs with HA

Nanoparticles were formulated using 15 mM $Ca^{2+}$ to 200 µL of DMEM buffered with 44 mM sodium bicarbonate (pH adjusted to 7.4), following the protocol described above (Development of CA NPs and particle size measurement section). The particles were subjected to further incubation for 10 min more in the presence of different concentrations (125 pM-1nM) of HA. The medium was added to make the total volume of 1 mL.

## Characterization of Formulated NPs by Using Fourier Transform Infrared (FTIR) Spectroscopy and Photo Thermal-infrared Spectroscopy (PT-IR)

FTIR spectroscopy was carried on by a Varian 640-IR over the wavenumber range 4000–400 $cm^{-1}$ as per protocol. The data extracted were analyzed by the Varian Resolution Pro 640 software (Agilent, Santa Clara, CA, USA). Both plain and hybrid HA-CA NPs were formulated by using 15 mM $Ca^{2+}$ in DMEM buffered with 44 mM bicarbonate following the same protocol described above (Development of CA NPs and particle size measurement section). The samples were centrifuged twice at 3200 rpm for 30 min. Then the supernatants were discarded. In the next step, small amounts of autoclaved Milli-Q water were added to the pellets. This centrifuge was conducted at 3200 rpm speed for 30 min to achieve the desired level of separation of the NPs without doing any harm to the particles. The pellets (that were precipitated) were kept at −20°C for 30 min and lyophilized as per protocol (Labconco, Kansas City, MO, USA) before performing the acquisition of IR spectra.

The hybrid nanoparticles were also prepared by using 15 mM $Ca^{2+}$ in DMEM buffered with 44 mM sodium bicarbonate and 500 pmol HA following the same protocol described above (Modification of NPs with HA section). The fabricated hybrid HA-NPs were centrifuged at 4000 rpm for 20 min and the precipitated pellets were lyophilized as per protocol by using a freeze dryer (Labconco, Kansas City, MO, USA).

## Characterization of Formulated NPs by Dynamic Light Scattering (DLS)

Both plain and hybrid nanoparticles were prepared by using 15 mM $Ca^{2+}$ in DMEM buffered with 44 mM concentration of the sodium bicarbonate in presence or absence of 500 pmol HA following the same protocol described above. The suspension was then as per protocol incubated at 37°C for 30 min, followed by mixing with 10% FBS. The formulations were then stored in the 4°C ice chiller during measurement. The DLS of NPs was then measured in 5.50 mm position at a refractive index (RI) of 1.330 and viscosity 0.8872 at 25°C by a Malvern Nano Zetasizer.

## Characterization of Formulated Hybrid NPs by Field Emission Scanning Electron Microscope (FE-SEM)

The particles of prepared samples were visualized through FE-SEM (HitachiS-4700 FE-SEM, Japan) at 10–15 kV. Nanoparticles were then centrifuged at 15,000 RPM for 10 min, followed by discarding the supernatant and resuspension of the resultant pellet with Milli-Q water. Salt particle suspensions were stored on ice until performing microscopic observation. One microliter of each sample was taken to place on carbon sample holder (tape coated) and dried at room temperature as per protocol, then followed by platinum sputtering of the dried samples for 30 s.

## Optical Profilometry Study of Plain and Hybrid Nanoparticles

Plain and hybrid nanoparticles were formulated by using 15 mM $Ca^{2+}$ in DMEM buffered with 44 mM sodium bicarbonate in presence or absence of 500 pmol HA following the same protocol described above. The formulated NPs as per protocol were then centrifuged at 4000 rpm for 20 min and the collected precipitated pellets were lyophilized by using a freeze dryer (Labconco, Kansas City, MO, USA). Then the particle distribution was analyzed using the Zeta-20 that measures and quantifies surface roughness.

## Binding Affinity Study of siRNA with Hybrid CA Nanoparticles

Particles with nanosize dimensions were tested based on their binding capabilities with fluorescence-labeled siRNA by fluorescence microscopy and with the help of a fluorescence plate reader. Subsequently, fluorescence-labeled siRNA/nanoparticles have been incubated with the MCF-7 cell lines for 1–4 h prior to observation by a fluorescence microscope. Thus, particles having high degree affinity to the siRNA molecules and the capacity for cellular level endocytosis have been selected for subsequent studies. Plain CA and hybrid CA NPs were formulated by using 15 mM $Ca^{2+}$ in DMEM buffered with 44 mM concentration of sodium bicarbonate in presence or presence of 500 pmol HA following the same protocol described in the above sections. 10 nM of the All Stars Negative siRNA (AF 488) (QIAGEN) was allowed to interact with plain and hybrid CA NPs at 37°C for 30 min. The prepared CA-siRNA complexes were then undergone to centrifuge at 13,000 rpm for 15 min as per protocol. The resulting pellets were then dissolved with 20 mM of EDTA in PBS. One hundred microliters of each sample was placed into a 96-well OptiPlate (Nunc) and the fluorescence intensity was determined by the 2030 multilabel reader VICTOR™ X5 (Perkin Elmer) and then analyzed using Perkin Elmer 2030 manager software with $\lambda ex = 490$ nm and $\lambda em = 535$ nm.

## Cellular Uptake Study of Fluorescence Labeled siRNA Bound to CAs and Hybrid CAs

For observing the cellular uptake property, 10 nM of the AF 488 neg. siRNA was conjugated with both NPs and hybrid NPs. NPs were formulated with 3 mM concentration of Ca salt as described above. After 30 min incubation at 37°C, 10% FBS-supplemented DMEM was then added to the suspension of NPs to stop their aggregation tendency if exists. MCF-7 cells were then protocol wise treated with these NPs-bound siRNA. After 4 h, the cells were washed with 5 mM EDTA in PBS to remove extracellular NPs and NP-bound siRNAs and observed under a fluorescent microscope (Olympus DP73).

In addition, the treated cells were washed with 5 mM EDTA in PBS and lysed before fluorescence intensity was measured for the lysate in 2030 multilabel reader VICTOR™ X5 (Perkin Elmer) and analyzed with integrated Perkin Elmer 2030 manager software using 490 nm and 535 nm wavelengths. Samples were then blank corrected using untreated samples. The experiment was then conducted in duplicate and expressed as mean ±SD. Statistical analysis was undertaken in different treatment groups.

## Cell Culture and Seeding Study

MCF-7 and 4T1 cells were grown in 25 $cm^2$ culture flask in DMEM with 10% FBS in a humidified atmosphere containing 5% $CO_2$ at 37°C. As per protocol, exponentially growing breast cancer cells were trypsinized, followed by mixing with fresh medium. The cell suspension was then centrifuged for 5 min and the supernatant was removed. Fresh medium was added to resuspend the pellets and the cells were counted by using a hemocytometer. Appropriate dilutions were done by properly using medium to produce a cell suspension with concentration $5.0\times10^4$ cells/mL. One milliliter of the prepared cell suspension was then added into each of the wells in a 24-well plate and incubated overnight at 37°C and 5% $CO_2$.

## In vitro Cytotoxicity Study of CA NPs and siRNA-loaded Hybrid CA NPs

MCF-7 cells with a density of $5\times10^4$ cells/well were seeded in a 24-well plate and each well contained 1 mL of DMEM (high glucose) supplemented with 10% FBS and a 1% penicillin-streptomycin solution. After the incubation at 37°C in a 5% $CO_2$ humid environment for 24 h, triplicate wells were treated within CA NPs formulated with different concentrations of $Ca^{2+}$ described in the above section. The treated MCF-7 cells were incubated for 48 h. The untreated cells were served as a blank control. The number of living cells was determined by MTT assay with 3-(4,5-dimethyl-thiazole-2-yl)-2,5-diphenyltetrazolium bromide. Microscopic images were also observed after 48 h of treatment. MTT assay was conducted at 48 h to ascertain the cell viability. A 48-h incubation period might be able to allow the cells in vitro to undergo desired multiple rounds of cell division with a view to providing a clearer picture of their growth and viability.

The fraction of the viable MCF-7 breast cancer cells after treatment with the NPs carrying the siRNAs against different ion channels and transporters was done by performing MTT assay. In short, 50 µL of MTT (5 mg/mL in PBS) was then added into each of the wells, by incubation at 37°C and 5% $CO_2$ for 4 h. After the incubation as per protocol, the medium containing MTT was aspirated and the purple formazan crystals at the bottom of each well were dissolved by mixing with 300 µL of DMSO solution. Then the absorbance of the resulting formazan solution was carried on spectrophotometrically at wavelength 595 nm using microplate reader Dynex Opsys MR, (Dynex Technologies, VA, USA) with reference to 630 nm. Each experiment was performed in triplicate and the data were plotted as mean ±SD of three independent experiments.

## In vivo Distribution Study of Modified CA Nanoparticles

Female Balb/c mice (6- to 8-weeks old) of 15–20 g of body weights (obtained from the university animal facility) were maintained under 12 h light:12 h dark cycles and provided with ab libitum feeding and water. All the experiments conducted were carried out as per the protocol approved by MONASH Animal Ethics Committee (MARP/2016/126). The guideline for handling animals which is based on Australian Animal Welfare Standards and Guidelines and follows the relevant Victorian and federal government legislation of Australia. Approximately, $1\times10^5$ 4T1 cells (in 100 µL PBS) were injected subcutaneously on the mammary pad. For conducting the biodistribution study, mice were administered with fluorescent (F)-siRNA (AF488) (1 mM) either free form or nanoparticle-bound form (prepared as discussed above section) through tail vein injection using 30 G needle after the tumor volume reached 13.20 ± 2.51 $mm^3$ on day 12. For the synthesis of CA particles, exogenous calcium salt was added at 15 mM to 200 µL of DMEM before incubation at 37°C for 30 min. For the modification of CA particles' surface, the formulated particles were subjected to further incubation for 10 min in the presence of 1 µL hyaluronic acid (HA).

All mice were sacrificed as per protocol by cervical dislocation following 4 and 24 h of treatment and various organs (brain, liver, kidney, liver, lung and spleen) as well as tumor were harvested immediately and washed twice with 1x chilled PBS. Then 1 mL prepared chilled lysis buffer per 500 gm of tissue mass was then added to the Eppendorf tube. The collected organs and tumors were then frozen at −80°C until further analysis was done following homogenization (Eppendorf, Germany). The homogenized lysate was centrifuged at 10,000 rpm for at least 15 min at 4°C. One hundred microliters of the centrifuged supernatant was then added to a 96-well black optiplate to measure the intensity of the fluorescence of AF 488-labeled siRNA with an excitation wavelength of 485 nm and an emission wavelength of 535 nm with the help of a 2030 multilabel reader Victor™ X5 (Perkin Elmer, USA).

## 4T1-induced Mouse Model of Breast Cancer and Antitumor Activity of siRNA-Loaded CA NPs

These experiments were conducted as per the protocol described in the above section. For the in vivo antitumor activity study, when the volume of the developed tumor reached at the level of an average of 39 $mm^3$ at approximately day 9 10, mice were then grouped on a random basis such as four mice per group. Then they were treated IV (intravenously) (tail-vein) at the right or left caudal vein. Then the second dose was administered 3 days after the first dose. The length and width of tumor outgrowth were determined by using the Vernier caliper in mm scale over a period of 24 days. The data subsequently was produced as mean ±SEM of the tumor volumes of each group. The volume of the tumor was calculated using on the formula mentioned below:

$$\text{Tumor Volume } (\text{mm3}) = {}^{1}/_{2}(\text{length} \times \text{width2}).$$

## Statistical Analysis

Results are produced as mean ±SD. Dunnett's test for 2-way ANOVA was performed using GraphPad Prism 7 to compare treatment groups (CA-loaded single siRNA and multiple siRNAs) and control group (untreated) in in vitro and in vivo biodistribution studies. Values were significant at $p$=0.01–0.05, very significant at $p$=0.001–0.01, extremely significant at $p$=0.0001–0.001, and extremely significant at $p$<0.0001.

# Results and Discussion

## Fabrication and Characterization of CA NPs by Enhancing Carbonate Substitution in the Apatite Structure

The diameter of NPs is an important determinant for their success of the endocytosis with bound siRNA. The growth in size of the CA NPs as a result of super saturation was carried out with varying concentrations[53–57] of calcium chloride, while the concentrations of other components- inorganic phosphate and carbonate were kept constant. Plain CA NPs were formulated using the protocol discussed in the methods section. As shown in Supplementary Figure 1, particle formation was enhanced with increasing $Ca^{2+}$ concentration, as represented by high turbidity. However, when we added DMEM buffered with 176 mM of bicarbonate to form the NPs, a tremendous drop in turbidity was observed. This could happen by higher incorporation of more carbonate ions into the crystal lattice as well as to minimize charges through interaction between $Ca^{2+}$ and excess bicarbonate/carbonate ions temporally. Thereby it might cause slowing down of the reaction rate for the generation of particles and reducing particle size even with increasing calcium ion concentration.

The size distribution of the nanocrystals formed was observed with respect to the percentage of the particles falling within 10 nm range and the variation in sizes for 90% (majority) of the particles (Supplementary Figures 2 and 3) by increasing the concentration of $Ca^{2+}$ in DMEM of high bicarbonate (176 mM). The turbidity and particle size analysis (Supplementary Figures 4 and 5) showed that in the DMEM prepared with high concentrations of bicarbonate (176 mM) and inorganic phosphate (1.5 mM), an increased level of turbidity was observed with increased particle sizes and then decreased, with increasing calcium concentration. The turbidity measurement (Supplementary Figure 4) of CA NPs was done at 320 nm with a UV spectrophotometer. The increasing turbidity indicates higher particle formation with concomitant increase in size and/or number of the particles, with only exception observed in case of 176 mM bicarbonate. The bicarbonate at 176 mM might have stopped the formation of even smaller crystals. Supplementary Figure 5 demonstrated that $Ca^{2+}$ affected particle formation. Higher concentration of $Ca^{2+}$ (Supplementary Figure 4) increased the turbidity, reflecting the higher particle formation accompanied by increased size and/or the number of the generated particles. Since calcium is a major constituent of CA, an increase in $Ca^{2+}$ concentration triggered more particle formation. The surface properties of CA having $Ca^{2+}$ and $PO_4^{3-}$-rich domains can enhance binding facility of either anionic or cationic macromolecules to the particles by electrostatic interactions.[7,57]

## Optical Microscopic Observation of NPs

The particles were used for the characterization not only by UV-VIS spectrophotometry but also by optical image analysis. The increasing concentration of any of the reactants results to increased particles' generation, and eventual self-aggregation for forming larger sized particles. There was the presence of high concentration of NaCl and glucose in DMEM and important to determine their functions in growing particles and stabilizing particles' size. The images (Supplementary Figure 6) of the particles formulated in various concentrations of $Ca^{2+}$ demonstrated that the aggregated particles formed with lower concentrations of $Ca^{2+}$ were enormously low, while the number of the particles gradually increased with higher concentrations of $Ca^{2+}$. When the concentration of $Ca^{2+}$ reached 35–45 mM, the NPs aggregated significantly, indicating that the high number of particles could lead to potential cytotoxicity.[7]

## Characterization of NPs by Fourier Transform-Infrared Spectroscopy (FT-IR)

The spectrum of CA NPs was determined by Varian FT-IR by using the Varian Resolution Pro 640 software (Agilent, Santa Clara, CA, USA) as per protocol to determine the peaks of carbonate and inorganic phosphate.

The FT-IR spectra (Supplementary Figure 7) generally demonstrated the formation of CA particles by identifying carbonate in the apatite material, as evident from the peaks between 1410 and 1540 $cm^{-1}$ and at approximately 880 $cm^{-1}$, as well as phosphate in the apatite, as shown by the peaks at 1000–1100 and 550–650 $cm^{-1}$. The formation of CA with different concentrations of bicarbonate salt was ensured by FT-IR. The FT-IR spectra of carbonate and phosphate were obtained. The spectra displayed peaks at 1410−1540 $cm^{-1}$ and 880 $cm^{-1}$ for $CO_3^{2-}$ and 1000–1100 $cm^{-1}$ and 550–650 $cm^{-1}$ for $PO_4^{3}$–. The overall vibration pattern suggests that CA was formed successfully.

## Characterization Study of NPs by Dynamic Light Scattering (DLS)

A Zetasizer was used to investigate the poly dispersing index (PDI) values of the NPs. The PDI values were determined for the dispersion and the homogeneity study of the particles. As shown in Table 2, the PDI values of NPs were less than 0.5, giving ideas about the homogeneous level of the distribution of particles. Particle size distribution study is expressed by number and volume and usually might have indicated variably sized particles.

Observing the lower PDI value of NPs suggests that particles have less tendency to become agglomerated with the formation of smaller and at the same time uniform distribution of particles. Many studies discussed that relatively small size particle distribution might show favorable pharmacokinetic profiles and could have the ability to enter into the target cancer cells more efficiently via the mechanism endocytosis.[57] The greater variation of SD resulted from the PDI values of the particles formulated with 176 mM bicarbonate salt might indicate their greater tendency to agglomerate forming big crystals. For all subsequent studies, 44 mM and 88 mM bicarbonate salts were used for particle fabrication.

## Characterization of NPs by Field Emission Scanning Electron Microscope (FE-SEM)

FE-SEM (Hitachi S-4700) was used to observe the morphology and actual size of the particles. From the images shown in Figure 2a and b, NPs formulated with 44 mM bicarbonate showed the spherical type shape having a rough surface and a homogeneous distribution pattern. The average diameter observed for the particles was within the range of 85–190 nm, demonstrating less tendency to self-aggregation. Conversely, NPs formed with 88 mM bicarbonate were found higher in number and smaller in size distribution (15–150 nm). It could be assumed that the smaller particle size was the effects of high concentration of bicarbonate salt in slowing down the reaction, preventing self-aggregation but leading to heterogeneous particles distribution. The homogeneous, smaller and rough surface NPs formed with 44 mM bicarbonate were likely to describe better ability to bind with the drug and less affinity to bind with the protein in systemic circulation.

## pH Sensitivity Studies of CA NPs

The efficiency in many cases of inorganic CA NPs-mediated siRNA drug therapy might depend largely on in time release of siRNA from the carrier. CA NPs-siRNA complexes after internalization into the targeted cell via the mechanism endocytosis might help the siRNA (payload) to escape from endosomes and thus, avoid lysosomal degradation. NPs could be dissolved in acidic endosomes and then they might be able to release the payload from the NPs. The dissolution of nanoparticles could also lead to accumulation of ions ($Ca^{2+}$, $PO_4^{3-}$ and $CO_3^{2-}$). Then they might further develop osmotic pressure across the membrane of the endosome. It might result in the breakdown of the endosome and there by cause releasing the therapeutics into the cytosol. As shown in Figure 3, decreasing the absorbance of different NPs formulations was observed with decreasing the pH. At the pH of 6.5, the NPs were noticed almost degraded when the

**Table 2** Comparison the Effects of Different Concentration of Exogenous Bicarbonate Salt in Fixed Exogenous Ca Salt on PDI Values

| Bicarbonate Salt Concentration | PDI Values | SD |
|---|---|---|
| 44 mM bicarbonate salt | 0.6 | 0.06 |
| 88 mM bicarbonate salt | 0.5 | 0.05 |
| 176 mM bicarbonate salt | 0.5 | 0.23 |

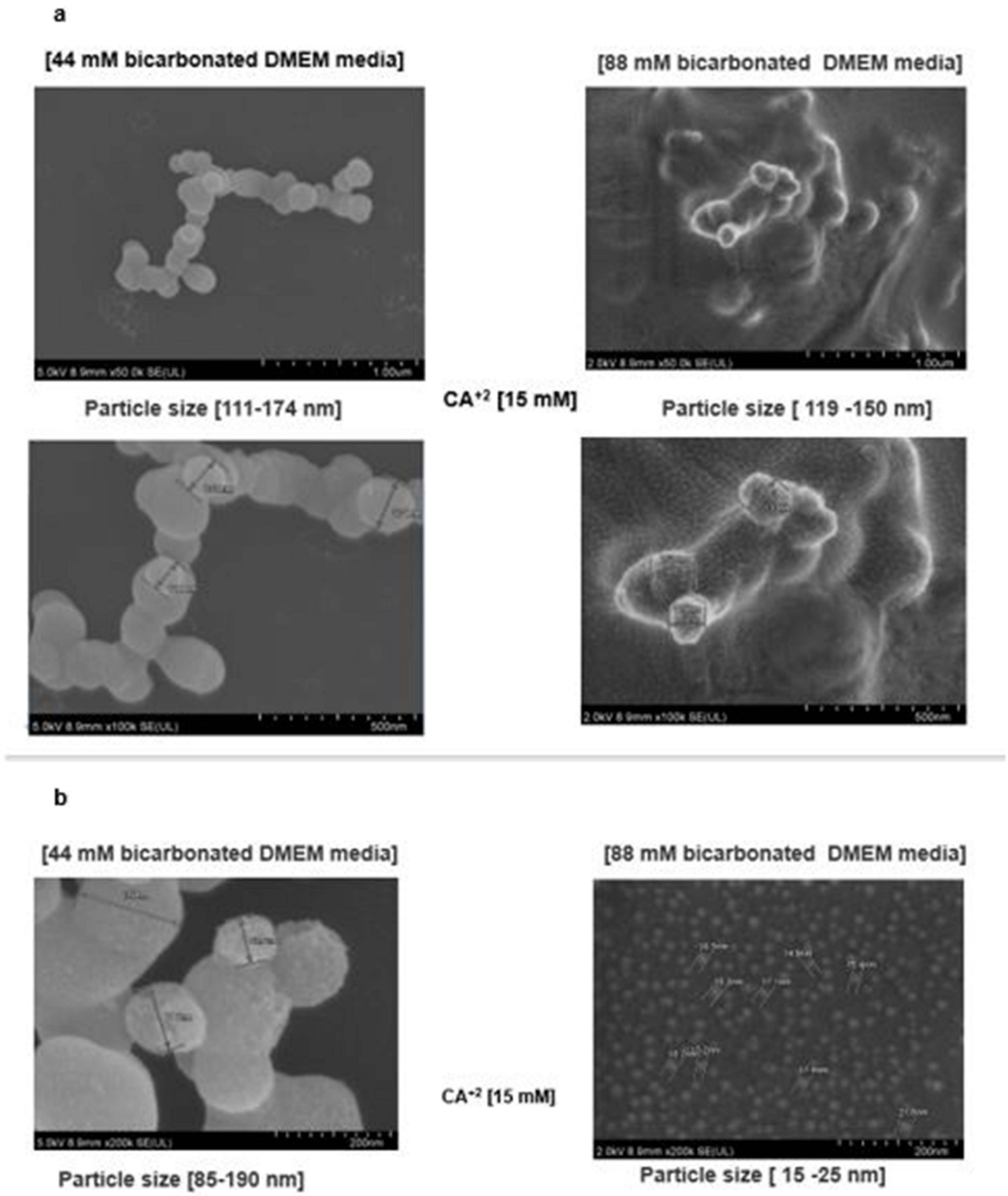


**Figure 2** NPs by Field Emission Scanning Electron Microscope (FE-SEM). Photos were captured at 100× magnification. Bar indicates 500 nm −1 μm scale (**a**) and 200 nm (**b**).

absorbance value was below 0.1 nm. The release was observed at pH 6.5 with a view to creating a simulated pH condition of the biological environment. The absorbance to express the release was determined as it could accurately quantify the concentration of the nanoparticles in the suspension. The result suggests that CA NPs were not stable at all

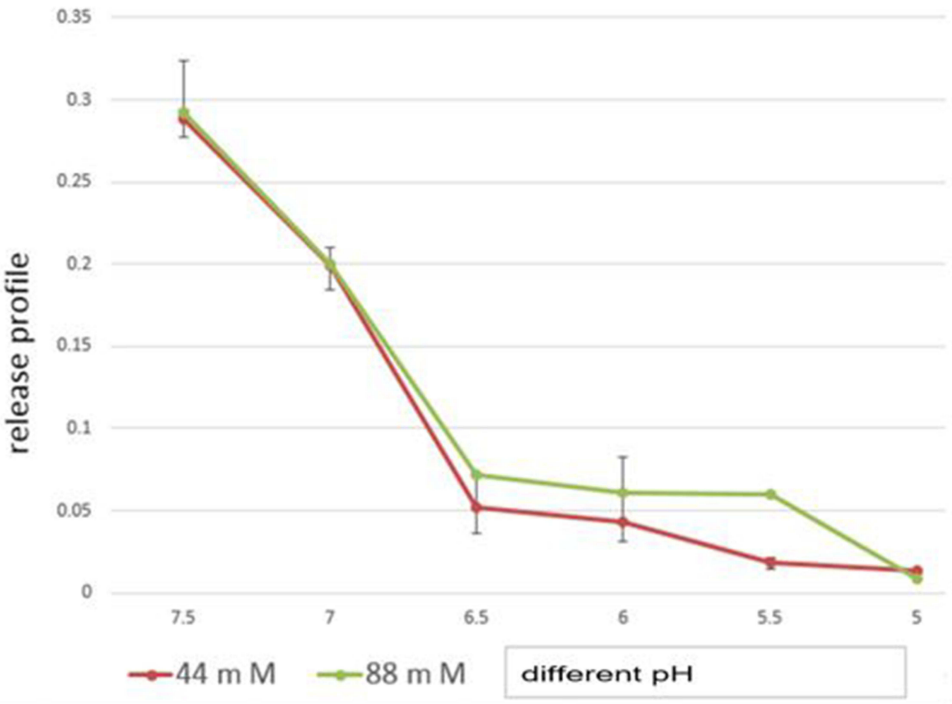


**Figure 3** pH-dependent release of CA NPs at pH 6.5–6.8 particles were fully degraded with an absorbance value <0.1, indicating the dissolution of CA NPs at acidic pH. This study proves the pH sensitivity of carbonate apatite nanoparticles (CA NPs).

and almost degraded in the acidic pH. Thus it might indicate that the dissolution of the particles may happen in the acidic environment of the endosomes and then they could facilitate early release of siRNA.

## Binding Affinity Study of siRNA to CA NPs

The MCF-7 cells were incubated with fluorescence-labeled siRNA/NPs complexes for 1–4 h prior to observation by a fluorescence microscope as shown in Figure 4a and b. Negative charges abundant on the backbone of the phosphate of siRNA could bind very efficiently with the CA NPs through ionic interactions as CA NPs have cationic $Ca^{2+}$ rich domains.[7] With 15 mM concentration of $Ca^{2+}$ used to formulated NPs, siRNA binding to them reached to a plateau level, indicating that the binding of siRNA to the NPs became saturated under a fixed siRNA concentration, while the particle

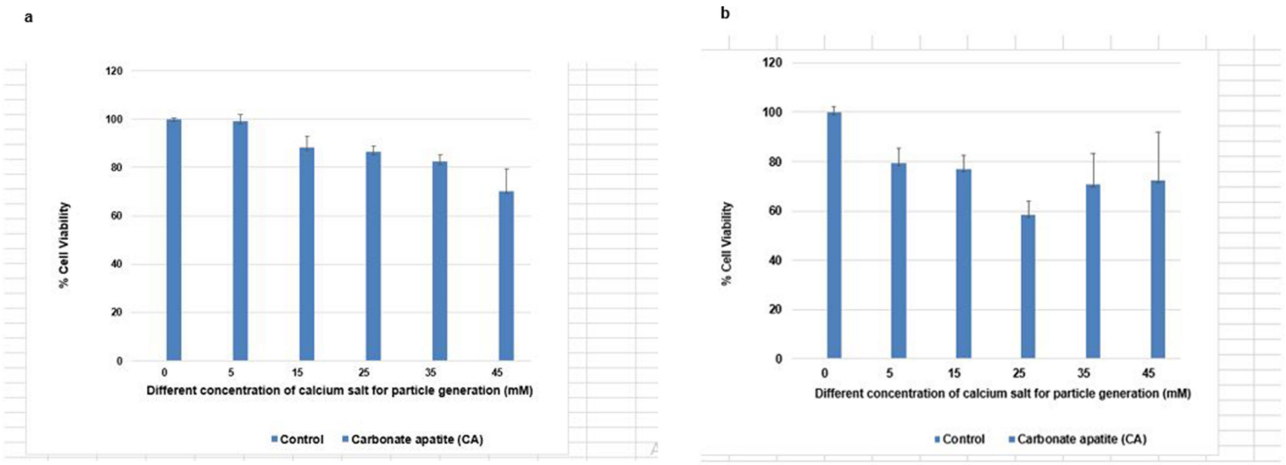


**Figure 4** Binding affinity studies of siRNA with CA nanoparticles. **(a)** represents 44 mM bicarbonated DMEM media with different concentration of Ca salt and **(b)** 88 mM bicarbonated DMEM media with different concentration of Ca salt.

size was still decreasing with a rise in $Ca^{2+}$ concentration. The particles might have aggregation tendency with higher concentration of $Ca^{2+}$ and these aggregated particles would provide limited siRNA binding sites as the surface area of the particles decreases with aggregation.[7,57]

## Cellular Uptake Study of Fluorescence-labeled siRNA Bound to CA NPs

For observing the cellular uptake under a fluorescent microscope (Olympus DP73), 10 nM of the AF 488 negative siRNA was conjugated with plain NPs and then the cells were treated with these complexes for 4 and 8 h (Supplementary Figures 8, 9 and 10).

Cellular uptake of siRNA, is a critical step to regulate as a whole silencing efficacy. It is extensively influenced by the binding affinity of the siRNA for NPs and the size of the particles. The smaller sized particles might have more cellular internalization in comparison to the larger sized ones. The MCF-7 cells were then treated with different formulations of CA NPs for 8 h before discarding the extracellular particles using EDTA and eventual fluorescence microscope observation. After 4 h of treatment, (as shown in Supplementary Figures 8, 9, and 10) NPs formulated with 88 mM bicarbonate were not able to show any significant signal of the fluorescence. Alternatively, cells treated with NPs formed with 44 mM bicarbonate showed significant fluorescence signal after 4 h. However, after 8 h of treatment, NPs formulated with 88 mM bicarbonate, coupled with siRNA conferred more significant fluorescence signal, indicating their successful internalization into the cells in the extended period of time (Figure 5). The results concluded that CA NPs formed in 44 mM bicarbonate buffer were more efficiently taken up by the cells via endocytosis than CA NPs formed with 88 mM bicarbonate after 4 h. The formulation with heterogeneous particles size distribution assumed to have adherence mainly to the cell membrane rather than going into the cells. This property of the particles might indicate that particle size and their distribution really matters to dramatically influence the cellular uptake.[7,57,58] Because of the efficient cellular uptake shown by the CA NPs developed with 44 mM bicarbonate salt, for the next studies involving the hybrid NPs, 44 mM bicarbonate salt was used.

## Development of Hybrid CA NPs with Hyaluronic Acid (HA) and Particle Size Measurement

Inorganic nanoparticles have been used in many ways to overcome the shortcomings of organic carriers in gene silencing study. They have some unique physicochemical properties. The biocompatibility and flexibility characteristics of inorganic nanoparticles could become more functionalized by using different ligands and also using coating materials

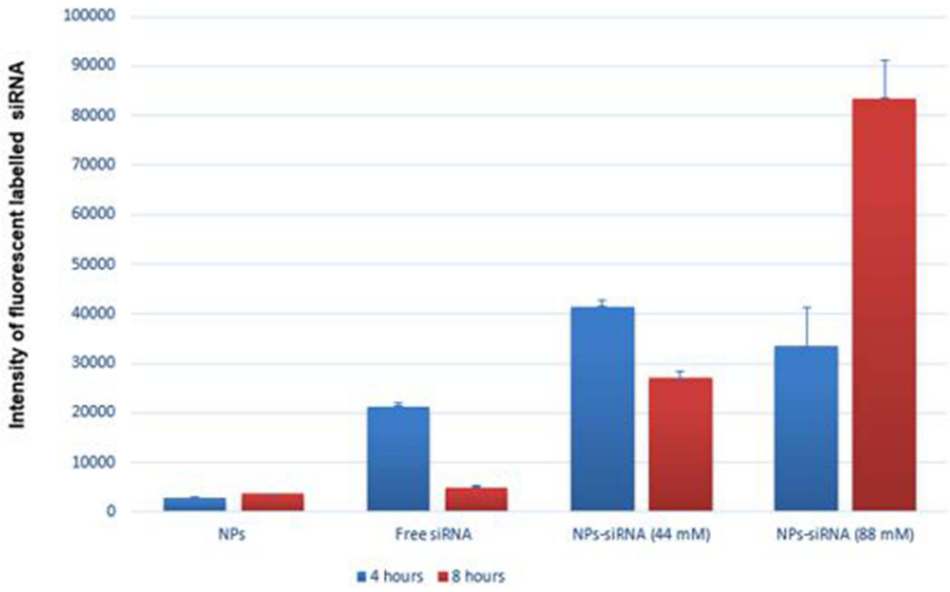


**Figure 5** Fluorescence intensity of intracellular components. Values are represented for duplicate samples compared to NPs treatment.

on the particles' surface, such as organic polymers HA. HA might have controlled more efficiently release kinetics of the particles and also show better compatibility with other potential therapeutic agents.[59–61]

Plain and hybrid CA NPs were formulated by using the protocol discussed in the method section. To ensure that the nanoparticle (NP) fabricated in this study successfully delivers the siRNA through endocytosis, the particle diameter is one the important determinants. The turbidity and particle size distribution of the hybrid HA-CA nanoparticles formed were observed (Figures 6 and 7). Dose-dependent HA might play a role in reducing particle size with fixed concentrations of bicarbonate and calcium ions. Particle size of surface modified CA NPs with HA could be largely dose dependent. The poly dispersity index (PDI) and zeta potentials values were also shown in Figures 8 and 9. The PDI values (<0.5) are considered for stable nanoparticles formation. The lowest concentrations of HA could result increased particles' aggregation due to the low electrostatic repulsion having PDI value with big error bars. NPs containing 500 pmol HA might have stable PDI making them stable due to having stronger electrostatic repulsion barrier.

## Characterization of NPs by Photo Thermal-Infrared Spectroscopy (PT-IR)

The PT-IR spectra[59] in the Figure 10 has demonstrated the formation of hybrid carbonate apatite particles by identifying carbonate in the apatite material, as evident from the peaks between 1410 and 1540 $cm^{-1}$ and at approximately 880 $cm^{-1}$

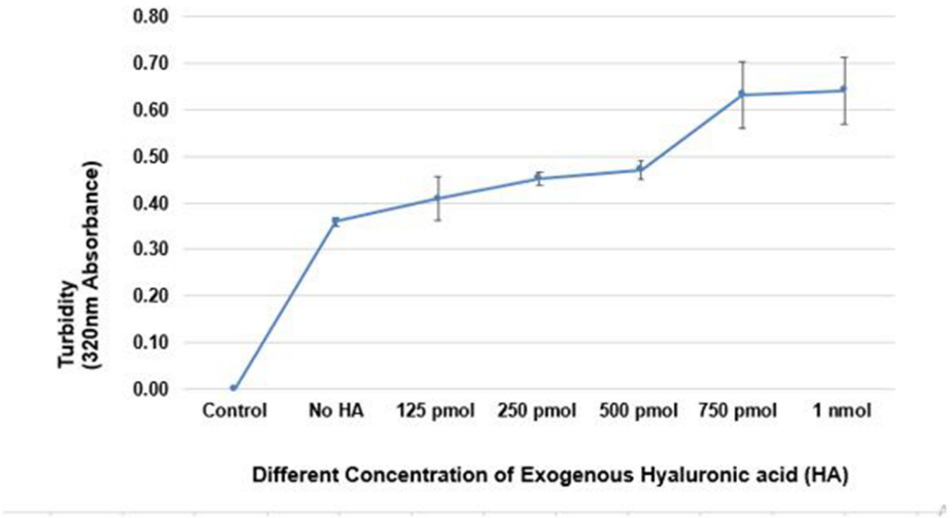


**Figure 6** Turbidity measurement of hybrid CA NPs by enhancing hyaluronic acid (HA). The data are presented as mean ±SD of triplicates.

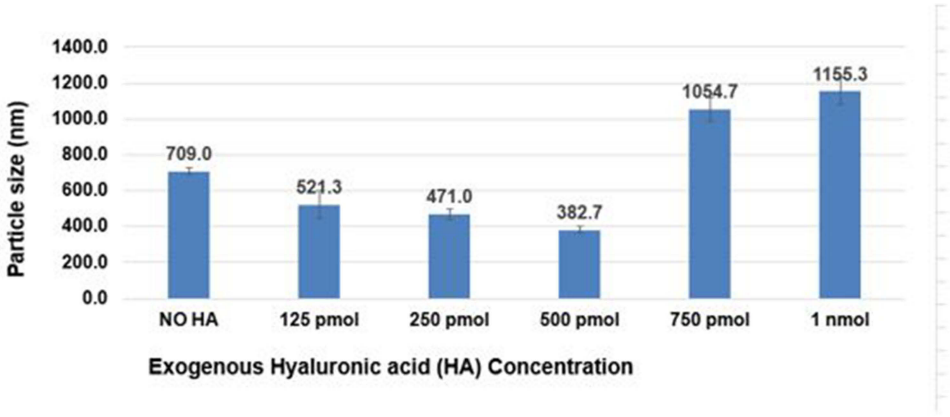


**Figure 7** Measurement of particle size of hybrid CA NPs by enhancing HA. Particles were analyzed by Zetasizer to measure average size. The data are displayed as mean ±SD of triplicate experiments.

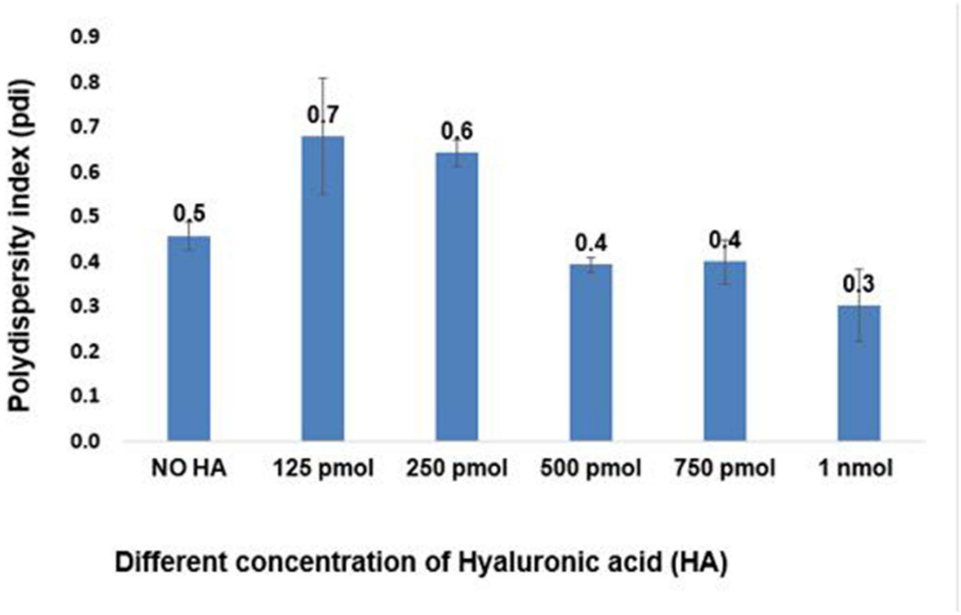


**Figure 8** Determination of PDI values. The data are displayed as mean ±SD of triplicate experiments.

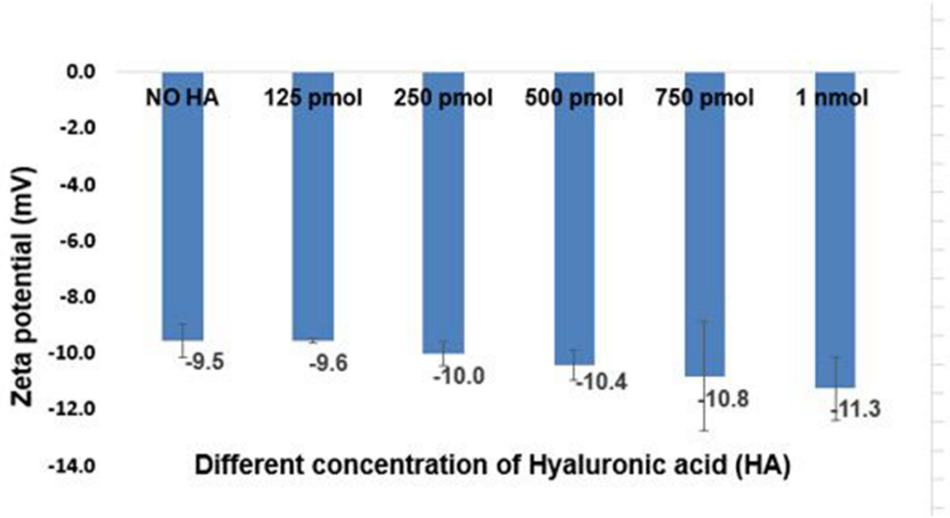


**Figure 9** Determination of Zeta Potentials (mV) The data are displayed as mean ±SD of triplicate experiments.

and phosphate in the apatite, as shown by the peaks at 1000–1100 $cm^{-1}$,[60] as well as 1600–1650 $cm^{-1}$ for O-H, C=0, N-H present in hyaluronic acid.[62] The broad and strong peaks at 1600–1650 $cm^{-1}$, confirmed the existence of the numerous carboxyl and hydroxyl groups in HA.

## Optical Profilometry Study of Plain and Hybrid CA NPs

It is extremely difficult to incorporate and disperse NPs, especially for a high percentage mainly due to the strong tendency of inorganic NP aggregation. The purpose of profilometry is to get the idea about the surface morphology (step heights/surface roughness/particles dispersion) of nanoparticles.

As shown in Figure 11, there was a significant enhancement of uniform particle formation upon addition of HA to CA NPs. Being polyanionic in nature, HA molecule might have efficiently interacted with $Ca^{2+}$-rich domains of CA NPs and induced repulsion among the neighboring particles through its multi-anionic charges present on the particle surface,

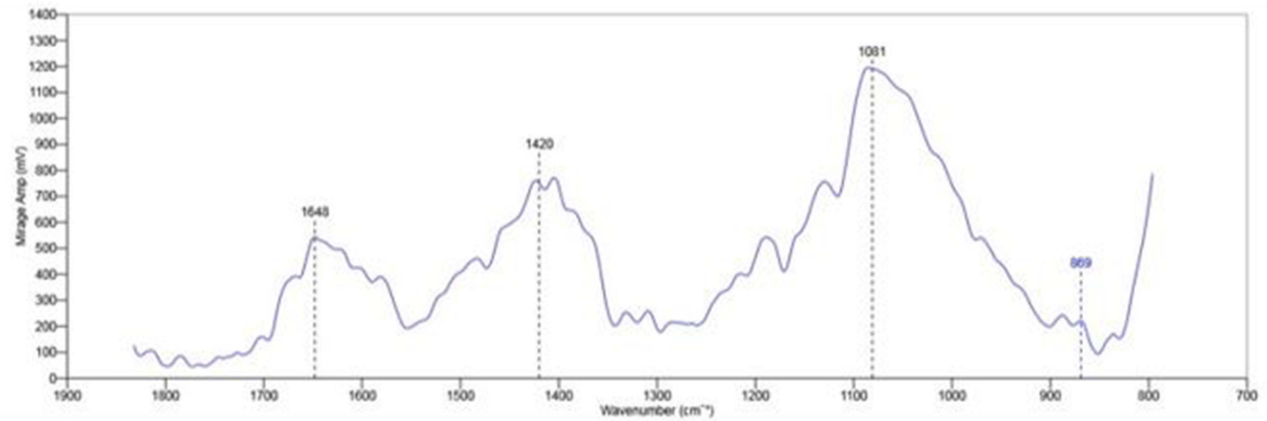


**Figure 10** The spectra displayed peaks at 1410–1540 $cm^{-1}$ and 880 $cm^{-1}$ for $CO_3^{2-}$, 1000–1100 $cm^{-1}$ for $PO^{4-}$ and 1600–1650 $cm^{-1}$ for O-H, C=0, N-H present in hyaluronic acid (HA).

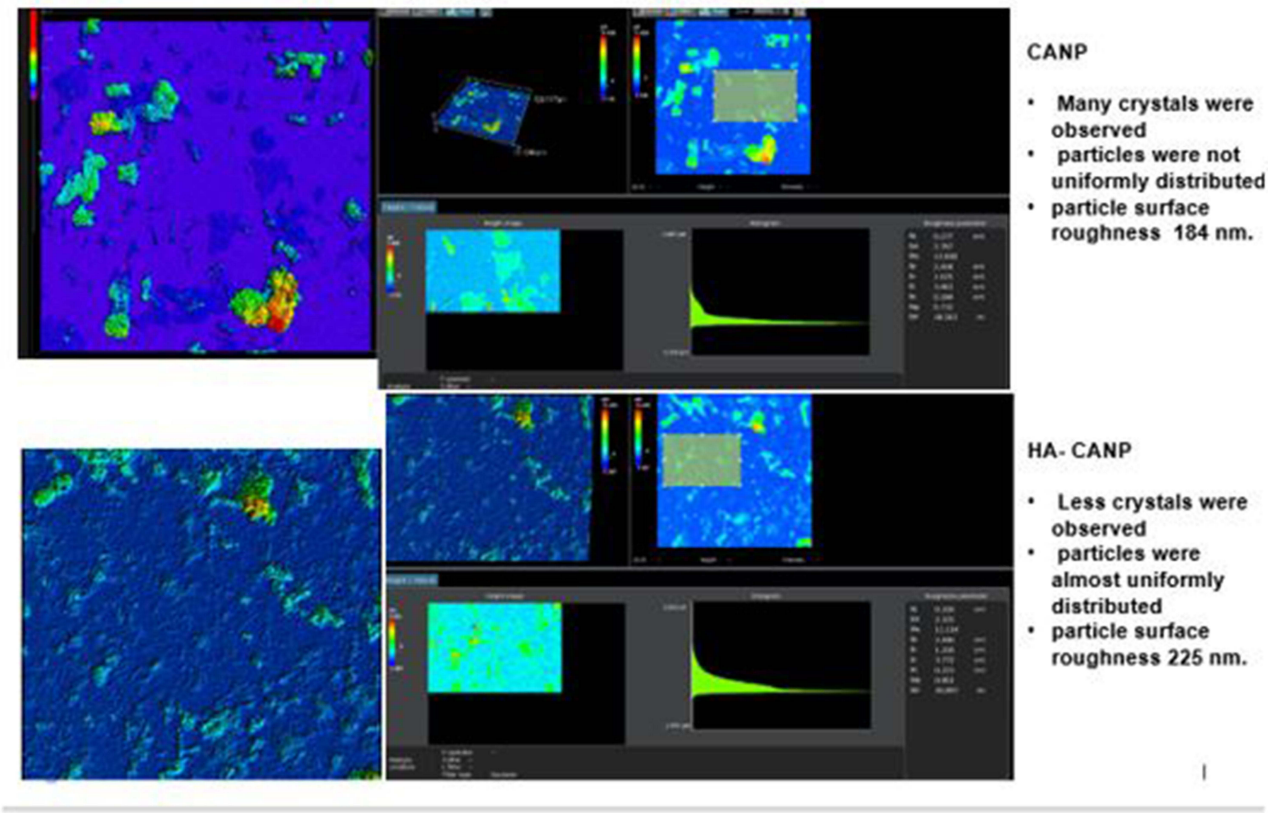


**Figure 11** Profilometry study to determine surface morphology (step heights/surface roughness) of nanoparticle.

thereby both stabilizing the particles and preventing their self-aggregation. Increasing the dose of HA resulted in unprecedented uniform distribution of the particles, supporting its potential role in repelling the surrounding particles.

## Cytotoxic Effects of Hybrid CA Carrying siRNAs Targeting TRPC6, TRPM8, and SLC41A1 Genes of MCF-7 Cells

MCF-7 cells were treated with hybrid HA-CA NPs carrying single and multiple siRNAs targeting *TRPC6*, *TRPM8*, and *SLC41A1* genes for a consecutive period of 2 days. HA-CAs were formulated with 44 mM bicarbonate, 15 mM $Ca^{2+}$ and

500 pM HA in the presence or absence of the siRNA(s). MCF-7 cells were treated with (i) media (untreated) (ii) NPs (iii) NPs+ siRNA complexes.

As shown in Figure 12, compared to the control (untreated or NP-treated cells), a greater and robust decrease in MCF-7 cell viability was observed. This decrease in cell viability was happened when siRNA targeting *TRPC6* or a combination of siRNAs targeting *TRPC6*, *TRPM8*, and *SLC41A1* were delivered intracellularly with HA-CA NPs. Treatment with *TRPC6* siRNA alone and in combination with two other siRNAs might significantly inhibit the pathways responsible for proliferation and survival of the cancer cells, focusing probable cross-talk(s) of those mentioned pathways with *TRPC6*, *TRPM8*, and *SLC41A1*.

## Antitumor Effect of Single and Multiple siRNAs Loaded Plain and Hybrid CA NPs

A widely used 4T1-induced murine breast cancer model was used to determine the effect of plain and HA-blended hybrid CA NPs carrying single and multiple siRNAs targeting *TRPC6*, *TRPM8*, and *SLC41A1* genes, on tumor regression. Treatments were administered twice within a 3-day interval through the tail vein, after the tumor volume reached 39 $mm^3$

The results of the tumor growth curve (Figure 13) showed that tumors grew fast almost in the same fashion as the control and NPs groups. In contrast, the growth of the tumor of the mice was treated with HA-CA NPs with single siRNA

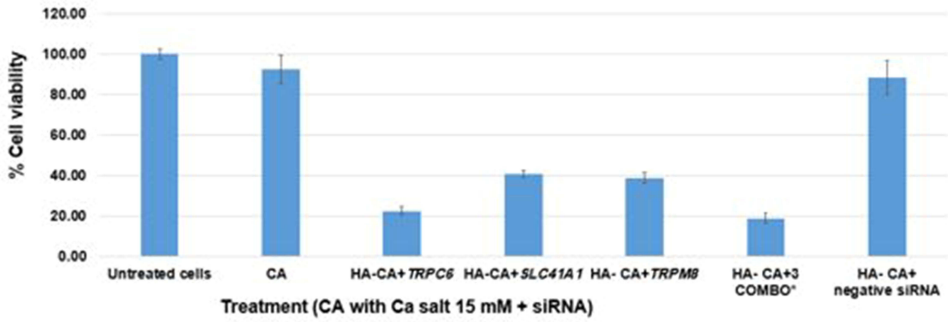


**Figure 12** Effects of intracellular delivery of single and three COMBO *(multiple siRNAs targeting *TRPC6*, *TRPM8*, and *SLC41A1*) genes using hybrid HA-CA NPs, on viability of MCF-7 cells. HA-CAs were formed in 44 mM bicarbonated DMEM with 15 mM $Ca^{2+}$ and 500 pM HA in presence or absence of the siRNA(s). Fifty thousand MCF-7 cells were seeded, treated the next day with empty HA-CA and siRNA(s)-loaded HA-CA NPs and incubated consecutively for 48 h. Subsequently, 50 μL of MTT was incorporated into the treated cells, with media containing MTT aspirated after 4 h incubation and 300 μL DMSO added subsequently. Spectrophotometric readings of viable cells were taken at 595 nm wavelength with reference of 630 nm.

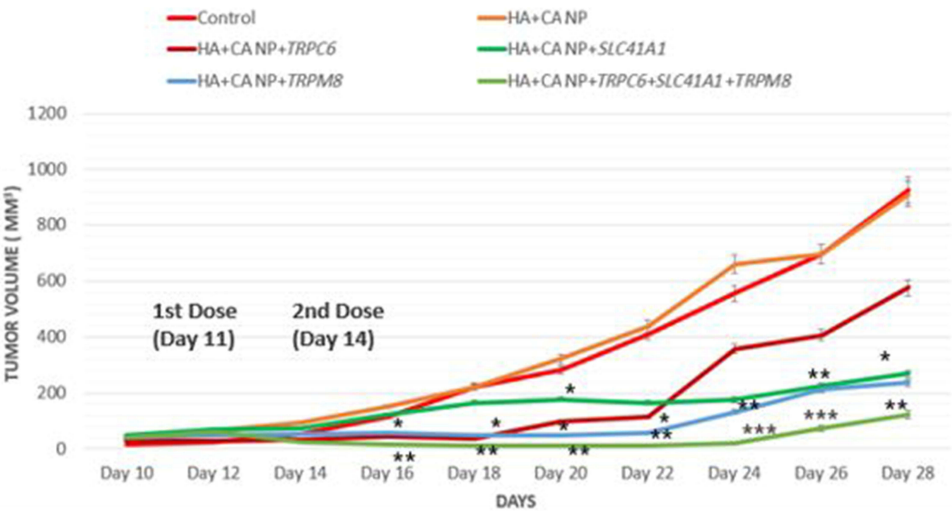


**Figure 13** Effects of IV (intravenous) administered nanoparticles and siRNA loaded nanoparticles on tumor regression. Tumor measurement by using a digital Vernier calliper (values are significant *$p<0.05$, very significant **$p<0.01$, and highly significant ***$p<0.001$).

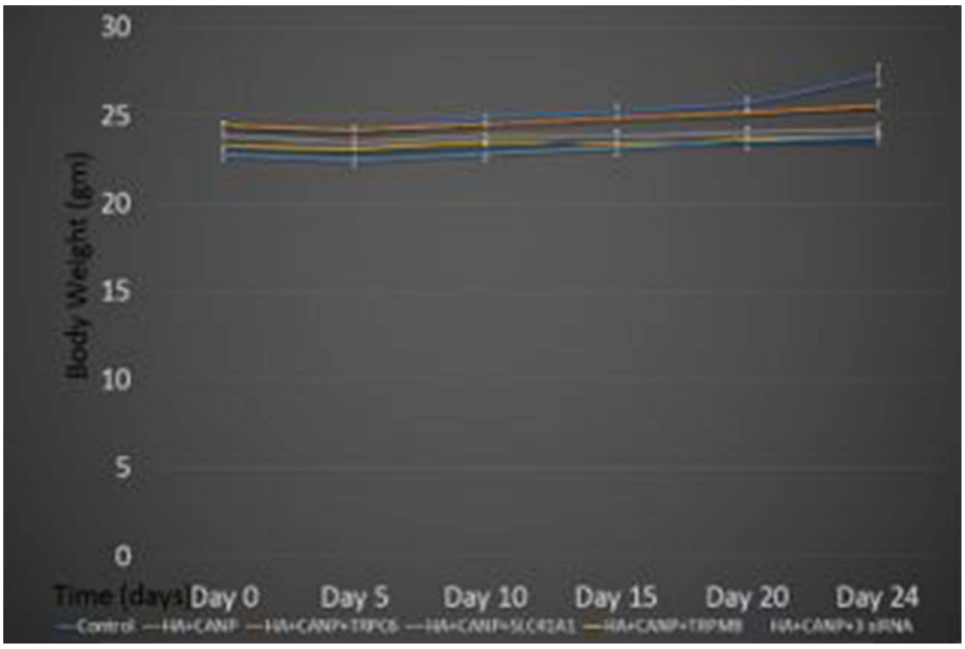


**Figure 14** Effects of IV administered nanoparticles and siRNA loaded nanoparticles on total body weight.

or multiple siRNAs. This treatment showed a comparatively slower rate of the growth and at the end smaller tumor volumes. These findings could demonstrate that hybrid NPs might have effectively reduced the growth of the tumor. However, the rate of inhibition of the tumor growth for triple siRNA(s) combination was more prominent than individual siRNA at the later stage, which could be explained by higher renal clearance and lower tumor accumulation of the latter. Out of the six injectable formulations, no one showed any kind of detrimental influence on the body weight of mouse (Figure 14). It might suggest that siRNA loaded nanoformulations might not have any acute toxic effects in mice on the time scale of the experiment. The significant antitumor effects of hybrid HA-CA NPs carrying siRNAs against the selective ion channel or transporter genes indicated that hybrid CA NPs could successfully protect the siRNA against the nuclease attack. They also ensure favorable pharmacokinetic profiles, induce no remarkable cytotoxicity, facilitate promising tumor uptake and last, but not the least, do rapid cytosolic release of the used siRNA(s).[60,63–65]

## Biodistribution Studies of Plain CA NPs and Hybrid HA-CA NPs

The biodistribution study as well as the tumor accumulation study of the siRNA were conducted by IV (intravenous) injection of the AF-488-siRNA conjugated CA NPs into mice bearing subcutaneous 4T1 tumor. After 24 h of the treatment, all the major organs and tumor were collected and the intensity level of the fluorescence was measured. The significant differences in the biodistribution and tumor accumulation of the siRNA. Therese significant differences were electrostatically connected with plain CA NPs and hybrid CA NPs were observed as shown in Figures 15 and 16.

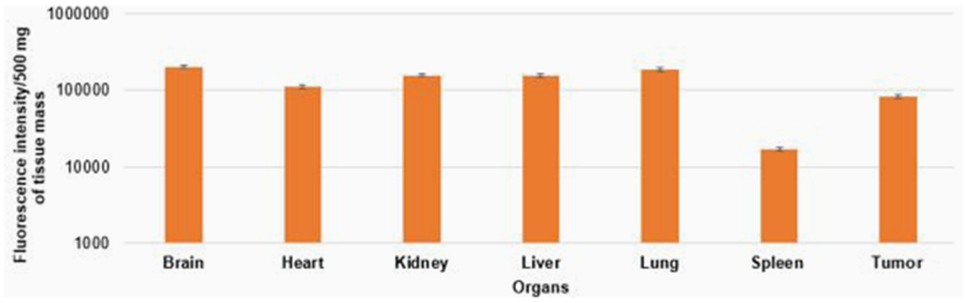


**Figure 15** Biodistribution studies of plain CA NPs after 24 h.

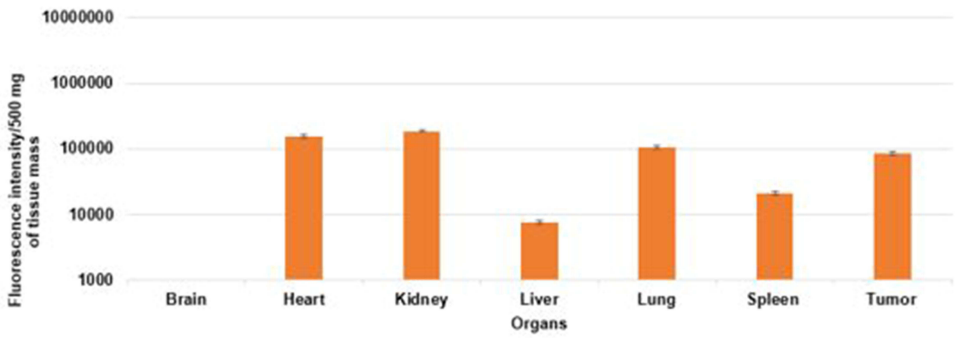


**Figure 16** Biodistribution studies of hybrid HA- CA NPs after 24 h.

The plain CA NPs were accumulated to a significant extent, in major organs (brain and heart), RES organs (liver, spleen) and urinary systems (Figure 15). Conversely, accumulation of hybrid HA-CA NPs was less in major organs compared to that of plain CA NPs except lungs (Figure 16) which displayed a higher degree of the fluorescence signals. This could be explained highlighting that smaller size distribution of the particles led faster renal clearance. This might be explained in a reverse way by increasing the hydrodynamic diameter by coating the CA NPs with HA. The accumulation of nanoparticles in the tumor cells largely depends on the physical and chemical properties of the particles. From the literature review it is established that the EPR effects as well as the vascular pore cutoff size ranging from 200 nm to 1.2 µm of tumors allow the nanoparticles to accumulate in the tumor cells more efficiently.[63,64] We found that the both plain and hybrid CA NPS facilitated a significant accumulation of the loaded siRNA in the tumor cells after 24 h of the treatment. There was a significant siRNA accumulation for both formulations in the off-target organs, such as brain, heart and lungs 24 h after the intravenous administration.[60,66]

## Conclusion

HA might have enhanced receptor (CD44)-mediated targeting of the siRNA-loaded hybrid NPs to the breast cancer cells. The biodegradable nature of the carrier might help efficient release of the delivered siRNAs via rapid self-dissolution in cellular acidic compartments (endosomes) following endocytosis. These findings thus suggest the potential applications of plain and hybrid CA NPs in efficiently delivering therapeutic siRNAs in clinical settings while revealing the tremendous prospect of targeting calcium ion channels and transporter genes in selectively killing breast cancer cells through delivery of the target genes-specific siRNAs using the developed NPs.

## Acknowledgments

The authors acknowledge the financial support received from the Ministry of Higher Education, Malaysia (MoHE) (FRGS/1/2018/STG05/MUSM/02/3).

## Disclosure

Ezharul Hoque Chowdhury is affiliated with Nanoflex LLC. The authors report no conflicts of interest in this work.

## References

1. Mansoori B, Shotorbani SS, Baradaran B. RNA interference and its role in cancer therapy. *Adv Pharm Bull*. 2014;4(4):313. doi:10.5681/apb.2014.046
2. Golan T, Khvalevsky EZ, Hubert A, et al. RNAi therapy targeting KRAS in combination with chemotherapy for locally advanced pancreatic cancer patients. *Oncotarget*. 2015;6(27):24560. doi:10.18632/oncotarget.4183
3. Kamaruzman NI, Aziz NA, Poh CL, Chowdhury EH. Oncogenic signaling in tumorigenesis and applications of siRNA nanotherapeutics in breast cancer. *Cancers*. 2019;11(5):632. doi:10.3390/cancers11050632
4. Stokłosa P, Borgström A, Kappel S, Peinelt C. TRP channels in digestive tract cancers. *Int J Mol Sci*. 2020;21(5):1877. doi:10.3390/ijms21051877
5. Roderick HL, Cook SJ. Ca2+ signalling checkpoints in cancer: remodelling Ca2+ for cancer cell proliferation and survival. *Nat Rev Cancer*. 2008;8(5):361–375. doi:10.1038/nrc2374
6. Monteith GR, Davis FM, Roberts-Thomson SJ. Calcium channels and pumps in cancer: changes and consequences. *J Biol Chem*. 2012;287(38):31666–31673. doi:10.1074/jbc.R112.343061

7. Uddin MB, Balaravi Pillai B, Tha KK, Ashaie M, Karim ME, Chowdhury EH. Carbonate apatite nanoparticles-facilitated intracellular delivery of siRNA (s) targeting calcium ion channels efficiently kills breast cancer cells. *Toxics*. 2018;6(3):34. doi:10.3390/toxics6030034
8. Zheng K, Yang Q, Xie L, et al. Overexpression of MAGT1 is associated with aggressiveness and poor prognosis of colorectal cancer. *Oncol Lett*. 2019;18(4):3857–3862. doi:10.3892/ol.2019.10710
9. Auwercx J, Rybarczyk P, Kischel P, et al. Mg2+ transporters in digestive cancers. *Nutrients*. 2021;13(1):210. doi:10.3390/nu13010210
10. Brini M, Carafoli E. Calcium pumps in health and disease. *Physiol Rev*. 2009;89(4):1341–1378. doi:10.1152/physrev.00032.2008
11. Nielsen N, Lindemann O, Schwab A. TRP channels and STIM/Orai proteins: sensors and effectors of cancer and stroma cell migration. *Br J Pharmacol*. 2014;171(24):5524–5540. doi:10.1111/bph.12721
12. Yang S, Zhang JJ, Huang X-Y. Orai1 and STIM1 are critical for breast tumor cell migration and metastasis. *Cancer Cell*. 2009;15(2):124–134. doi:10.1016/j.ccr.2008.12.019
13. Flourakis M, Lehen'Kyi VY, Beck B, et al. Orai1 contributes to the establishment of an apoptosis-resistant phenotype in prostate cancer cells. *Cell Death Dis*. 2010;1(9):e75–e75. doi:10.1038/cddis.2010.52
14. Faouzi M, Hague F, Potier M, Ahidouch A, Sevestre H, Ouadid-Ahidouch H. Down-regulation of Orai3 arrests cell-cycle progression and induces apoptosis in breast cancer cells but not in normal breast epithelial cells. *J Cell Physiol*. 2011;226(2):542–551. doi:10.1002/jcp.22363
15. Hiroshi T; Decreased miR-340 expression in bone marrow is associated with liver metastasis of colorectal cancer [*Doctoral Dissertation*]. Osaka University; 2014.
16. Saeed H, Iqtedar M. Stem cell function and maintenance–ends that matter: role of telomeres and telomerase. *J Biosci*. 2013;38(3):641–649. doi:10.1007/s12038-013-9346-3
17. Ito M, Kawano K, Miyagishi M, Taira K. Genome-wide application of RNAi to the discovery of potential drug targets. *FEBS Lett*. 2005;579 (26):5988–5995. doi:10.1016/j.febslet.2005.08.015
18. Chodon D, Guilbert A, Dhennin-Duthille I, et al. Estrogen regulation of TRPM8 expression in breast cancer cells. *BMC Cancer*. 2010;10(1):1–8. doi:10.1186/1471-2407-10-212
19. Shapovalov G, Ritaine A, Skryma R, Prevarskaya N. Role of TRP ion channels in cancer and tumorigenesis. In: *Seminars in Immunopathology*. Springer; 2016:357–369.
20. Guilbert A, Gautier M, Dhennin-Duthille I, et al. Transient receptor potential melastatin 7 is involved in oestrogen receptor-negative metastatic breast cancer cells migration through its kinase domain. *Eur J Cancer*. 2013;49(17):3694–3707. doi:10.1016/j.ejca.2013.07.008
21. Sahni J, Nelson B, Scharenberg AM. SLC41A2 encodes a plasma-membrane Mg2+ transporter. *Biochem J*. 2007;401(2):505–513. doi:10.1042/BJ20060673
22. Sahni J, Scharenberg AM. The SLC41 family of MgtE-like magnesium transporters. *Mol Aspect Med*. 2013;34(2–3):620–628. doi:10.1016/j.mam.2012.05.012
23. Zhao J, Mi Y, Feng -S-S. siRNA-based nanomedicine. *Nanomedicine*. 2013;8(6):859–862. doi:10.2217/nnm.13.73
24. Kesharwani P, Gajbhiye V, Jain NK. A review of nanocarriers for the delivery of small interfering RNA. *Biomaterials*. 2012;33(29):7138–7150. doi:10.1016/j.biomaterials.2012.06.068
25. Kutsuzawa K, Maruyama K, Akiyama Y, Akaike T, Chowdhury E. Efficient transfection of mouse embryonic stem cells with cell-adhesive protein-embedded inorganic nanocarrier. *Anal Biochem*. 2008;1(372):122–124. doi:10.1016/j.ab.2007.06.033
26. Corbo C, Molinaro R, Parodi A, Toledano Furman NE, Salvatore F, Tasciotti E. The impact of nanoparticle protein Corona on cytotoxicity, immunotoxicity and target drug delivery. *Nanomedicine*. 2016;11(1):81–100. doi:10.2217/nnm.15.188
27. Kumar A, Bicer EM, Morgan AB, et al. Enrichment of immunoregulatory proteins in the biomolecular Corona of nanoparticles within human respiratory tract lining fluid. *Nanomedicine*. 2016;12(4):1033–1043. doi:10.1016/j.nano.2015.12.369
28. Carvalho MP, Costa EC, Miguel SP, Correia IJ. Tumor spheroid assembly on hyaluronic acid-based structures: a review. *Carbohydr Polym*. 2016;150:139–148. doi:10.1016/j.carbpol.2016.05.005
29. Thapa R, Wilson GD. The importance of CD44 as a stem cell biomarker and therapeutic target in cancer. *Stem Cells Int*. 2016;2016:1–15. doi:10.1155/2016/2087204
30. Xu H, Tian Y, Yuan X, et al. The role of CD44 in epithelial–mesenchymal transition and cancer development. *Onco Targets Ther*. 2015;8:3783–3792. doi:10.2147/OTT.S95470
31. Inoue K, Fry EA. Aberrant splicing of estrogen receptor, HER2, and CD44 genes in breast cancer. *Genet Epigenet*. 2015;7:GEG. S35500. doi:10.4137/GEG.S35500
32. Lau WM, Teng E, Chong HS, et al. CD44v8-10 is a cancer-specific marker for gastric cancer stem cells. *Cancer Res*. 2014;74(9):2630–2641. doi:10.1158/0008-5472.CAN-13-2309
33. Kousar K, Naseer F, Abduh MS, Anjum S, Ahmad T. CD44 targeted delivery of oncolytic Newcastle disease virus encapsulated in thiolated chitosan for sustained release in cervical cancer: a targeted immunotherapy approach. *Front Immunol*. 2023;14:1175535. doi:10.3389/fimmu.2023.1175535
34. Kesharwani P, Chadar R, Sheikh A, Rizg WY, Safhi AY. CD44-targeted nanocarrier for cancer therapy. *Front Pharmacol*. 2022;12:800481. doi:10.3389/fphar.2021.800481
35. Zhang M, Ma Y, Wang Z, et al. A CD44-targeting programmable drug delivery system for enhancing and sensitizing chemotherapy to drug-resistant cancer. *ACS Appl Mater Interfaces*. 2019;11(6):5851–5861. doi:10.1021/acsami.8b19798
36. Naseer F, Kousar K, Abduh MS, Anjum S, Ahmad T. Evaluation of the anticancer potential of CD44 targeted vincristine nanoformulation in prostate cancer xenograft model: a multi-dynamic approach for advanced pharmacokinetic evaluation. *Cancer Nanotechnol*. 2023;14(1):65. doi:10.1186/s12645-023-00218-2
37. Eliaz RE, Szoka FC. Liposome-encapsulated doxorubicin targeted to CD44: a strategy to kill CD44-overexpressing tumor cells. *Cancer Res*. 2001;61(6):2592–2601.
38. Liang Y, Wang Y, Wang L, et al. Self-crosslinkable chitosan-hyaluronic acid dialdehyde nanoparticles for CD44-targeted siRNA delivery to treat bladder cancer. *Bioact Mater*. 2021;6(2):433–446. doi:10.1016/j.bioactmat.2020.08.019
39. Hussein HA, Abdullah MA. Novel drug delivery systems based on silver nanoparticles, hyaluronic acid, lipid nanoparticles and liposomes for cancer treatment. *Appl Nanosci*. 2022;12(11):3071–3096. doi:10.1007/s13204-021-02018-9

40. Yang X, Shang P, Ji J, et al. Hyaluronic Acid-Modified Nanoparticles Self-Assembled from Linoleic Acid-Conjugated Chitosan for the Codelivery of miR34a and Doxorubicin in Resistant Breast Cancer. *Mol Pharmaceut*. 2021;19(1):2–17. doi:10.1021/acs.molpharmaceut.1c00459
41. Pan C, Zhang T, Li S, et al. Hybrid nanoparticles modified by hyaluronic acid loading an HSP90 inhibitor as a novel delivery system for subcutaneous and orthotopic colon cancer therapy. *Int j Nanomed*. 2021;Volume 16:1743–1755. doi:10.2147/IJN.S275805
42. Chen C, Fan R, Wang Y, et al. Hyaluronic acid-conjugated nanoparticles for the targeted delivery of cabazitaxel to CD44-overexpressing glioblastoma cells. *J Biomed Nanotechnol*. 2021;17(4):595–605. doi:10.1166/jbn.2021.3050
43. Du W, Yang X, He S, et al. Novel hyaluronic acid oligosaccharide-loaded and CD44v6-targeting oxaliplatin nanoparticles for the treatment of colorectal cancer. *Drug Delivery*. 2021;28(1):920–929. doi:10.1080/10717544.2021.1914777
44. Wang W, Zhang X, Li Z, et al. Dendronized hyaluronic acid-docetaxel conjugate as a stimuli-responsive nano-agent for breast cancer therapy. *Carbohydr Polym*. 2021;267:118160. doi:10.1016/j.carbpol.2021.118160
45. Hu H, Zhang Y, Ji W, et al. Hyaluronic acid-coated and Olaparib-loaded PEI− PLGA nanoparticles for the targeted therapy of triple negative breast cancer. *J Microencapsul*. 2022;39(1):25–36. doi:10.1080/02652048.2021.2014586
46. Wang R, Yang H, Khan AR, et al. Redox-responsive hyaluronic acid-based nanoparticles for targeted photodynamic therapy/chemotherapy against breast cancer. *J Colloid Interface Sci*. 2021;598:213–228. doi:10.1016/j.jcis.2021.04.056
47. Xu R, Zhang K, Liang J, Gao F, Li J, Guan F. Hyaluronic acid/polyethyleneimine nanoparticles loaded with copper ion and disulfiram for esophageal cancer. *Carbohydr Polym*. 2021;261:117846. doi:10.1016/j.carbpol.2021.117846
48. Parayath NN, Hong BV, Mackenzie GG, Amiji MM. Hyaluronic acid nanoparticle-encapsulated microRNA-125b repolarizes tumor-associated macrophages in pancreatic cancer. *Nanomedicine*. 2021;16(25):2291–2303. doi:10.2217/nnm-2021-0080
49. Ghosh S, Dutta S, Sarkar A, Kundu M, Sil PC. Targeted delivery of curcumin in breast cancer cells via hyaluronic acid modified mesoporous silica nanoparticle to enhance anticancer efficiency. *Colloids Surf B*. 2021;197:111404. doi:10.1016/j.colsurfb.2020.111404
50. Thummarati P, Suksiriworapong J, Sakchaisri K, Junyaprasert VB. Effect of chemical linkers of curcumin conjugated hyaluronic acid on nanoparticle properties and in vitro performances in various cancer cells. *J Drug Delivery Sci Technol*. 2021;61:102323. doi:10.1016/j.jddst.2021.102323
51. Lai H, Ding X, Ye J, Deng J, Cui S. pH-responsive hyaluronic acid-based nanoparticles for targeted curcumin delivery and enhanced cancer therapy. *Colloids Surf B*. 2021;198:111455. doi:10.1016/j.colsurfb.2020.111455
52. Yu S, Wang S, Xie Z, et al. Hyaluronic acid coating on the surface of curcumin-loaded ZIF-8 nanoparticles for improved breast cancer therapy: an in vitro and in vivo study. *Colloids Surf B*. 2021;203:111759. doi:10.1016/j.colsurfb.2021.111759
53. Mozar FS, Chowdhury EH. Surface-modification of carbonate apatite nanoparticles enhances delivery and cytotoxicity of gemcitabine and anastrozole in breast cancer cells. *Pharmaceutics*. 2017;9(2):21. doi:10.3390/pharmaceutics9020021
54. S Mozar F, H Chowdhury E. Gemcitabine interacts with carbonate apatite with concomitant reduction in particle diameter and enhancement of cytotoxicity in breast cancer cells. *Curr Drug Deliv*. 2015;12(3):333–341. doi:10.2174/1567201812666150120153809
55. Tiash S, Othman I, Rosli R, Hoque Chowdhury E. Methotrexate-and cyclophosphamide-embedded pure and strontiumsubstituted carbonate apatite nanoparticles for augmentation of chemotherapeutic activities in breast cancer cells. *Curr Drug Deliv*. 2014;11(2):214–222. doi:10.2174/15672018106661312111019
56. Ibnat N, Islam RA, Chowdhury EH. Inhibition of breast tumour growth with intravenously administered PRKCA siRNA-and PTEN tumour suppressor gene-loaded carbonate apatite nanoparticles. *Appl Sci*. 2021;11(17):8133. doi:10.3390/app11178133
57. Ibnat N, Chowdhury EH. Retarding breast tumor growth with nanoparticle-facilitated intravenous delivery of BRCA1 and BRCA2 tumor suppressor genes. *Sci Rep*. 2023;13(1):536. doi:10.1038/s41598-022-25511-9
58. Chowdhury E. Nuclear targeting of viral and non-viral DNA. *Expert Opin Drug Delivery*. 2009;6(7):697–703. doi:10.1517/17425240903025744
59. Hossain SM, Shetty J, Tha KK, Chowdhury EH. α-Ketoglutaric acid-modified carbonate apatite enhances cellular uptake and cytotoxicity of a Raf-Kinase inhibitor in breast cancer cells through inhibition of MAPK and PI-3 kinase pathways. *Biomedicines*. 2019;7(1):4. doi:10.3390/biomedicines7010004
60. Hossain SM, Zainal Abidin SA, Chowdhury EH. Krebs cycle intermediate-modified carbonate apatite nanoparticles drastically reduce mouse tumor burden and toxicity by restricting broad tissue distribution of anticancer drugs. *Cancers*. 2020;12(1):161. doi:10.3390/cancers12010161
61. Mehbuba Hossain S, Chowdhury EH. Citrate-and succinate-modified carbonate apatite nanoparticles with loaded doxorubicin exhibit potent anticancer activity against breast cancer cells. *Pharmaceutics*. 2018;10(1):32. doi:10.3390/pharmaceutics10010032
62. Loh XJ, Lee T-C, Dou Q, Deen GR. Utilising inorganic nanocarriers for gene delivery. *Biomater Sci*. 2016;4(1):70–86. doi:10.1039/C5BM00277J
63. Karim ME, Shetty J, Islam RA, Kaiser A, Bakhtiar A, Chowdhury EH. Strontium sulfite: a new pH-responsive inorganic nanocarrier to deliver therapeutic siRNAs to cancer cells. *Pharmaceutics*. 2019;11(2):89. doi:10.3390/pharmaceutics11020089
64. Karim ME, Tha KK, Othman I, Borhan Uddin M, Chowdhury EH. Therapeutic potency of nanoformulations of siRNAs and shRNAs in animal models of cancers. *Pharmaceutics*. 2018;10(2):65. doi:10.3390/pharmaceutics10020065
65. Chowdhury EH. *Nanotherapeutics: From Laboratory to Clinic*. CRC press; 2016.
66. Shim MS, Kwon YJ. Efficient and targeted delivery of siRNA in vivo. *FEBS J*. 2010;277(23):4814–4827. doi:10.1111/j.1742-4658.2010.07904.x